

## ***Supporting Information***

**Promoting oxygen reduction reaction kinetics through manipulating electron redistribution in CoP/Cu<sub>3</sub>P@NC for aqueous/flexible Zn-air batteries**

Lixia Wang <sup>a</sup>, Jiasui Huang <sup>a</sup>, Jia Huang <sup>a</sup>, Bowen Yao <sup>a</sup>, Aling Zhou <sup>a</sup>, Zhiyang Huang <sup>a</sup>,  
Tayirjan Taylor Isimjan<sup>c,\*</sup>, Bao Wang,<sup>b,\*</sup> & Xiulin Yang <sup>a,\*</sup>

<sup>a</sup> *Guangxi Key Laboratory of Low Carbon Energy Materials, School of Chemistry and Pharmaceutical Sciences, Guangxi Normal University, Guilin 541004, China*

<sup>b</sup> *State Key Laboratory of Biochemical Engineering, Institute of Process Engineering, Chinese Academy of Sciences, Beijing 100190, China*

<sup>c</sup> *Saudi Arabia Basic Industries Corporation (SABIC) at King Abdullah University of Science and Technology (KAUST), Thuwal 23955-6900, Saudi Arabia*

E-mail: xlyang@gxnu.edu.cn, baowang@ipe.ac.cn, isimjant@sabic.com

† Electronic supplementary information (ESI) available. See DOI: <https://doi.org/>

10.1039/d3gcxxxxxx.

## **Materials characterization**

The phase determination of all samples was completed using an X-ray powder diffractometer (Rigaku D/Max-3c) with Cu K $\alpha$  radiation ( $\lambda=0.15418$  nm) to determine the composition. Raman spectra were measured with a Raman micro-spectrometer (Renishaw in Via Quotation) to determine the degree of graphitization of all samples. The laser wavelength was set to 785 nm with an initial power of 100 mW, which was set to 1% (1 mW) during the test, and the scanning range from 1000 to 2000  $\text{cm}^{-1}$ . A scanning electron microscopy (SEM, Quanta FEG 200, Holland) and a transmission electron microscope (TEM, Talos F200S) were used to investigate the microstructures of the as-prepared specimens. Energy-dispersive X-ray (EDX) spectroscopy was conducted to analyze the composition. The materials' Brunner-Emmett-Taylor (BET) surface area and pore size distribution were analyzed using a Quantachrome instrument (3H-2000PS4). The Barrett-Joyner-Halenda (BJH) method was used for pore size analysis. The element and surface valence states of the materials were measured with an ESCALAB 250Xi. The water contact angle was measured using a contact angle meter (JC2000D, China). The Four Probe Measurement uses the RTS-9 Dual Electro-Measurement Tester to analyze the resistivity and conductivity of samples.

## **Electrochemical measurements**

The electrochemical experiments were conducted by using a standard three-electrode system on a CHI760E electrochemical station at room temperature. The three-electrode system comprising a graphite rod as counter electrode, an Ag/AgCl (saturated KCl solution) was utilized as the reference electrode and a working electrode. The rotating ring disk electrode (RRDE, diameter = 5.61 mm, PINE instruments, USA) and rotating disk electrode (RDE,

diameter = 5 mm, PINE instruments, USA) loaded with catalyst ink served as the working electrode. 2 mg of the prepared electrocatalysts were ultrasonically dispersed in a mixed solution of 200  $\mu\text{L}$  isopropanol, 100  $\mu\text{L}$  deionized water, and 5  $\mu\text{L}$  5 wt% Nafion for 30 min to prepare suspension. Take 20  $\mu\text{L}$  of the catalyst ink was deposited onto the surface of RRDE, and dried naturally in the environment (loading:  $0.52 \text{ mg cm}^{-2}$ ). To ensure consistent loading, 16  $\mu\text{L}$  of dispersion was applied in RDE testing. The electrocatalytic activity of benchmark Pt/C catalyst (loading:  $0.1 \text{ mg cm}^{-2}$ ) was evaluated using the same method as a reference. The measured potential was calibrated to the standard reversible hydrogen electrode (RHE) potential from the Nernst equation in 0.1 M KOH to address pH deviations and ensure accuracy:

$$E_{RHE} = E_{Ag/AgCl} + 0.059\text{pH} + 0.196$$

Prior to measurement,  $\text{O}_2$  or  $\text{N}_2$  was passed into the 0.1M KOH solution for 30 minutes to saturate the electrolyte. The RHE calibration was conducted in  $\text{H}_2$ -saturated 0.1 M KOH solution using Pt plates as the working and counter electrodes, along with an Ag/AgCl electrode as the reference electrode (Fig. S1). Cyclic voltammetry (CV) curves were recorded in  $\text{O}_2/\text{N}_2$  saturated 0.1 M KOH solution at a scan rate of  $50 \text{ mV s}^{-1}$ . Linear sweep voltammetry (LSV) was performed at a range of -0.9 to 0.2 V at a scan rate of  $10 \text{ mV s}^{-1}$ , where the disk electrode speed was 1600 rpm (RDE and RRDE). The voltage applied to the Pt ring during the RRDE test was 1.464 V vs. RHE. In this study, the LSV data were processed by subtracting the current values under  $\text{O}_2$ -saturated conditions from those under  $\text{N}_2$ -saturated conditions, and then dividing by the area of the RDE/RRDE to obtain the current density.

The long-term stability was evaluated via chronoamperometry in  $\text{O}_2$ -saturated 0.1 M

KOH solution at a rotational velocity of 1600 rpm and a potential of 0.8 V vs. RHE. The Tafel slopes were derived from the Tafel equation:<sup>1,2</sup>

$$\eta = b \log_{10} \left( \frac{j}{j_0} \right)$$

Koutecky-Levich (K-L) equation was used to calculate the number of electron transfers ( $n$ ) in ORR process:

$$\frac{1}{j} = \frac{1}{j_k} + \frac{1}{j_L} = \frac{1}{j_k} + \frac{1}{B\omega^{1/2}}$$

$$B = 0.62nFC_0\nu^{-1/6}D_0^{2/3}$$

The  $j$  is the measured current density,  $j_k$  is the kinetic diffusion current density, and  $j_L$  is the limiting current density ( $\text{mA cm}^{-2}$ ),  $B$  is the reciprocal of the slope of the K-L plot,  $\omega$  is the angular velocity of the electrode ( $\omega=2\pi N$ ,  $N$  is the rotation speed),  $n$  is the electron transfer number for oxygen reduction,  $F$  is the Faraday constant ( $96485 \text{ C mol}^{-1}$ ),  $C_0$  is the saturated concentration of  $\text{O}_2$  ( $1.2 \times 10^{-3} \text{ mol L}^{-1}$ ),  $D_0$  is the diffusion coefficient of  $\text{O}_2$  ( $1.9 \times 10^{-5} \text{ cm}^2 \text{ s}^{-1}$ ), and  $\nu$  is the kinetic viscosity ( $0.01 \text{ cm}^2 \text{ s}^{-1}$ ).

RRDE measurements were conducted to investigate the hydrogen peroxide ( $\text{H}_2\text{O}_2$ ) yield (%) and electron transfer number ( $n$ ) of the catalysts and the values were calculated by the following equations:

$$n = 4 \frac{I_d}{I_d + I_r/N}$$

$$\text{H}_2\text{O}_2 (\%) = 200 \frac{I_r/N}{I_d + I_r/N}$$

Where  $I_d$  denotes the disk current,  $I_r$  is the ring current, and  $N$  is the current collection efficiency of the ring ( $N=0.37$ ).

### **Aqueous Zn-air batteries (ZAB) fabrication and test**

The home-made liquid Zn-air batteries (ZABs) were assembled by using polished zinc foil as the anode, aqueous solution containing 6 M KOH+0.2 M Zn(Ac)<sub>2</sub> as the electrolyte, and the catalyst coated on carbon paper as the air cathode. 2 mg of CoP/Cu<sub>3</sub>P@NC or commercial Pt/C was dispersed in a mixture of 200  $\mu$ L ethanol, 200  $\mu$ L deionized water, and 5  $\mu$ L 5 wt% Nafion, and sonicated for 30 min. The slurry was then applied onto a 1 cm  $\times$  1 cm hydrophilic carbon paper. The total catalyst loading amount on carbon paper was 2.0 mg cm<sup>-2</sup> for both CoP/Cu<sub>3</sub>P@NC and commercial Pt/C. The open circuit voltage (OCV) and charge-discharge polarization curves were acquired with an electrochemical workstation (CHI 760E). For cycling stability test, the cathodes were fabricated by mixing CoP/Cu<sub>3</sub>P@NC and RuO<sub>2</sub> with a mass ration of 2/1. For comparison, Pt/C+RuO<sub>2</sub> were also used to fabricate the cathodes of ZABs. The galvanostatic charge-discharge cycling stability for the ZABs was performed using a RAND battery test system (BT2016A) and CHI 760E at a current density of 5 mA cm<sup>-2</sup> for 20 min at each charge/discharge cycle.

The specific capacity was calculated according to the following equation:

$$\text{Specific capacity} = \frac{\text{discharge current} \times \text{time}}{\text{weight of consumed Zinc}}$$

### **Assembly of flexible solid-state ZAB**

The preparation of the catalyst ink was identical to that of the Zn-air battery, with CoP/Cu<sub>3</sub>P@NC and Pt/C loaded at 2 mg cm<sup>-2</sup>. The catalyst-coated carbon cloth, zinc foil, and polyvinyl alcohol hydrogel (PVA gel) electrolyte served as the cathode, anode, and solid

electrolyte, respectively, while nickel foam acted as the current collector to construct the flexible solid-state zinc-air battery. The solid-state electrolyte was synthesized as follows: First, 5 g of polyvinyl alcohol (PVA) was dissolved in 50 mL of deionized water and stirred at 90 °C for 1 hour to form a gel polymer electrolyte. Then, 5 mL of a mixed solution containing 18 M KOH and 0.02 M  $\text{Zn}(\text{CH}_3\text{COO})_2$  was added, and stirring continued for an additional 30 minutes. Finally, the resulting paste was frozen at -20 °C to obtain a solid electrolyte and later thawed at room temperature for further use.

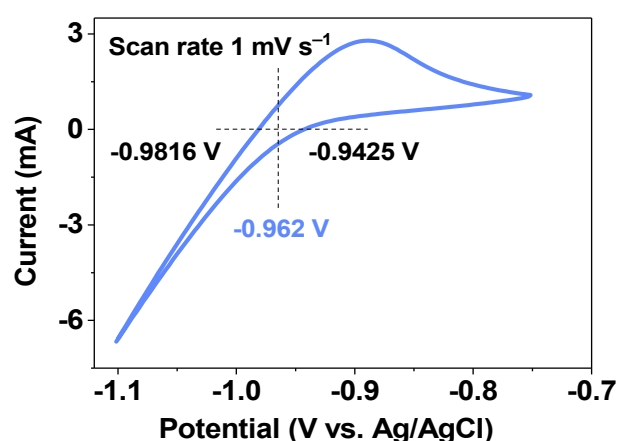


**Fig. S1.** The RHE calibration of saturated Ag/AgCl electrode in 0.1 M KOH. The average value of potential at zero current is regarded as the thermodynamic potential for hydrogen electrode reaction.

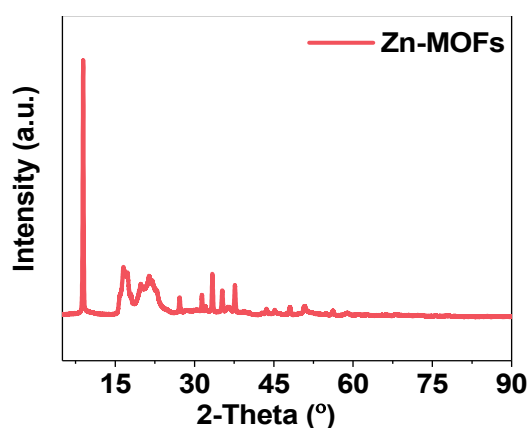


**Fig. S2.** XRD pattern of Zn-MOFs.

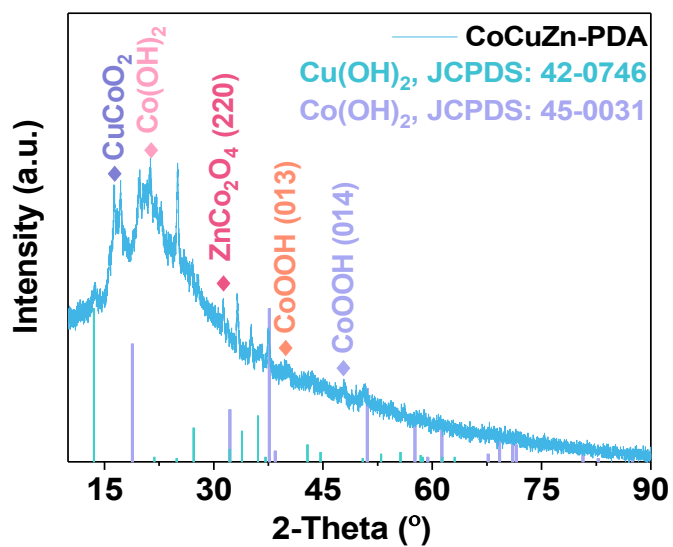


Fig. S3. XRD pattern of CoCuZn-PDA.

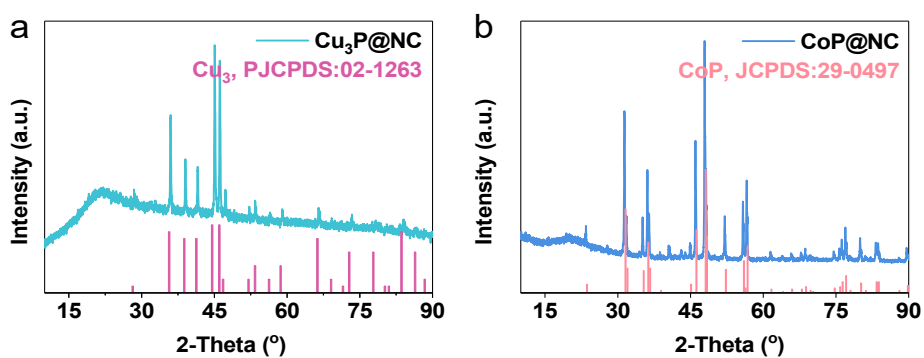


Fig. S4. XRD patterns of (a) Cu<sub>3</sub>P@NC, and (b) CoP@NC.

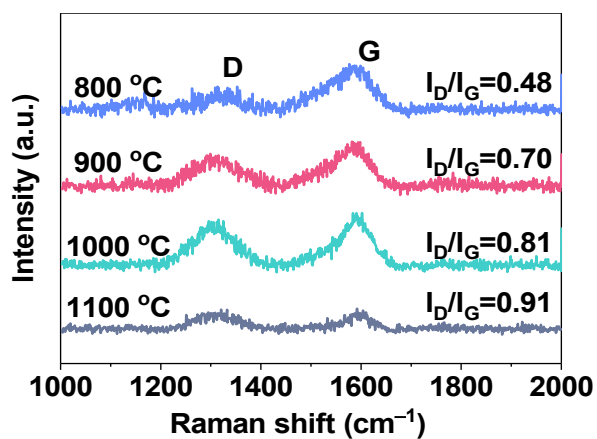


Fig. S5. Raman spectra of CoP/Cu<sub>3</sub>P@NC at different calcination temperatures.

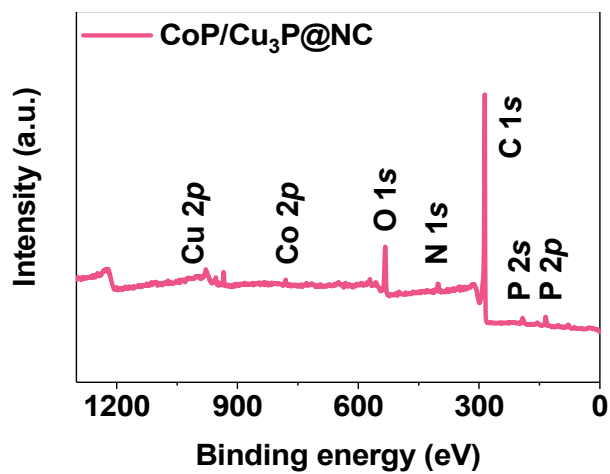


Fig. S6. XPS survey spectrum of CoP/Cu<sub>3</sub>P@NC.

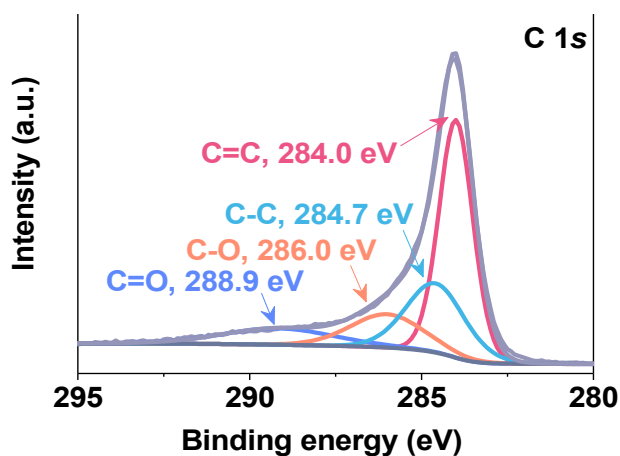
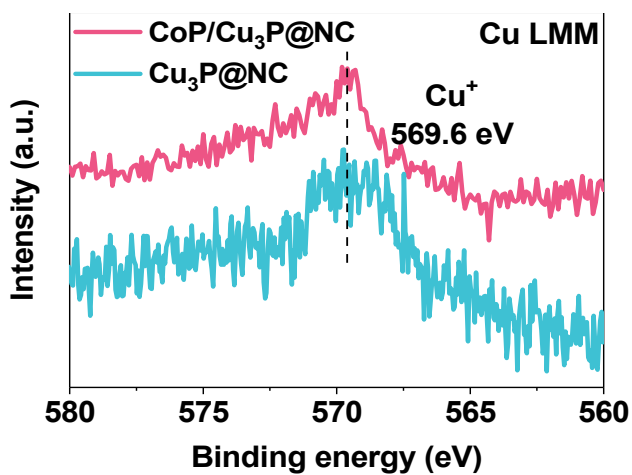
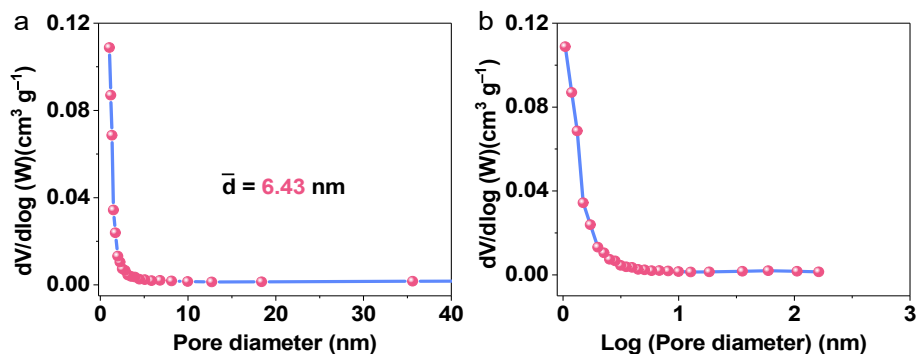


Fig. S7. High-resolution XPS spectrum of C 1s region in CoP/Cu<sub>3</sub>P@NC.



**Fig. S8.** Cu (LMM) Auger spectrum of the CoP/Cu<sub>3</sub>P@NC and Cu<sub>3</sub>P@NC.



**Fig. S9.** (a) The pore size distribution, (b) X-axis is plotted on a logarithmic scale of pore size distribution for CoP/Cu<sub>3</sub>P@NC.

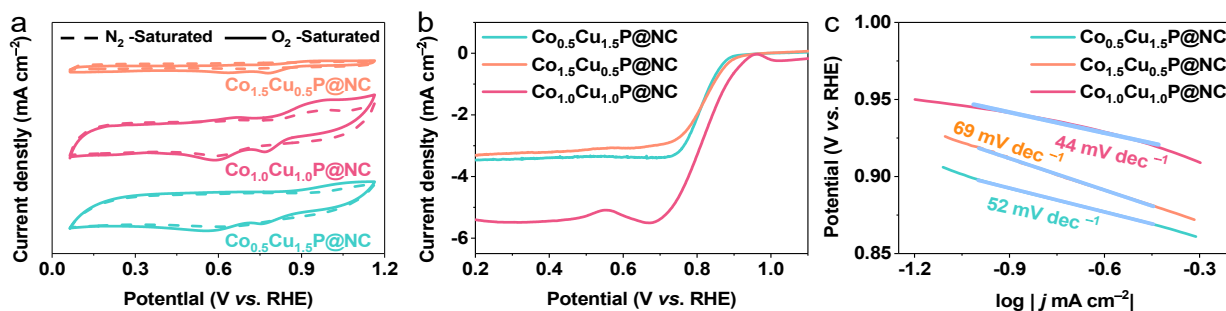


**Fig. S10.** (a) CV curves, (b) LSV polarization curves, and (c) Tafel plots of CoP/Cu<sub>3</sub>P@NC for different Co/Cu molar ratios.

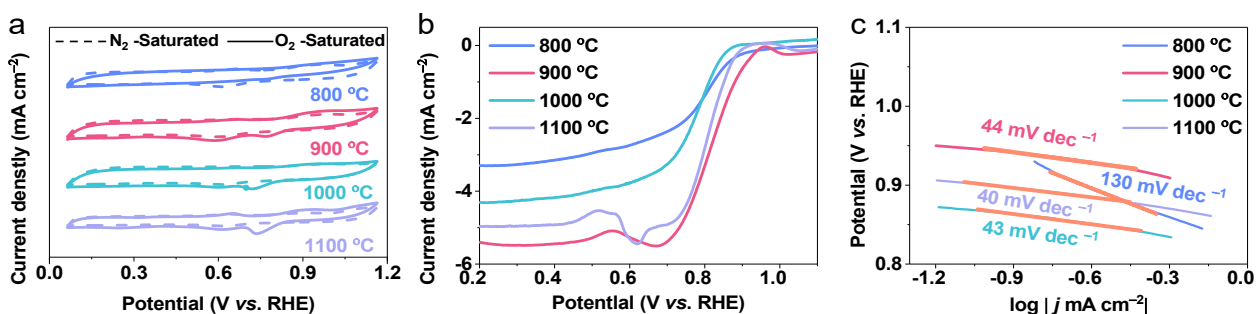


**Fig. S11.** Catalysts obtained at different calcination temperatures. (a) CV curves, (b) LSV polarization curves, and (c) Tafel plots.

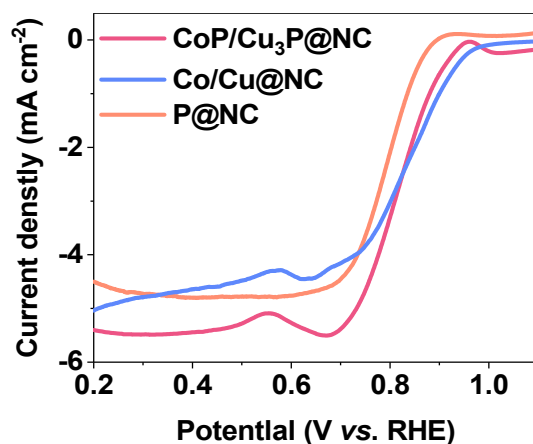


**Fig. S12.** LSV polarization curves of CoP/Cu<sub>3</sub>P@NC, CoCu@NC and P@NC catalysts.

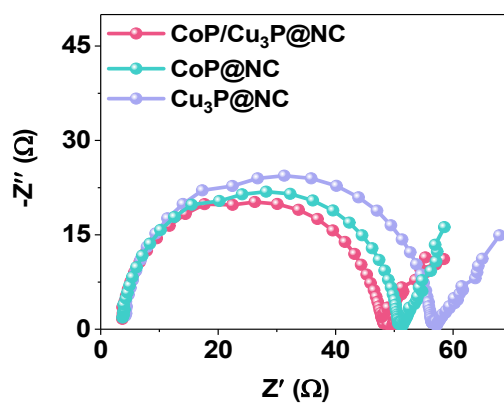


**Fig. S13.** Electrochemical impedance spectroscopy of CoP/Cu<sub>3</sub>P@NC, CoP@NC, and Cu<sub>3</sub>P@NC.

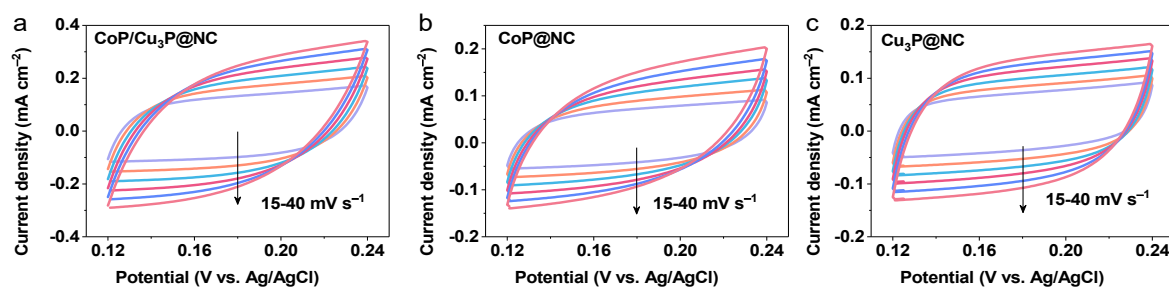


**Fig. S14.** CV curves of (a) CoP/Cu<sub>3</sub>P@NC, (b) CoP@NC, and (c) Cu<sub>3</sub>P@NC at various scan rates in the non-Faradaic region to test  $C_{dl}$ .

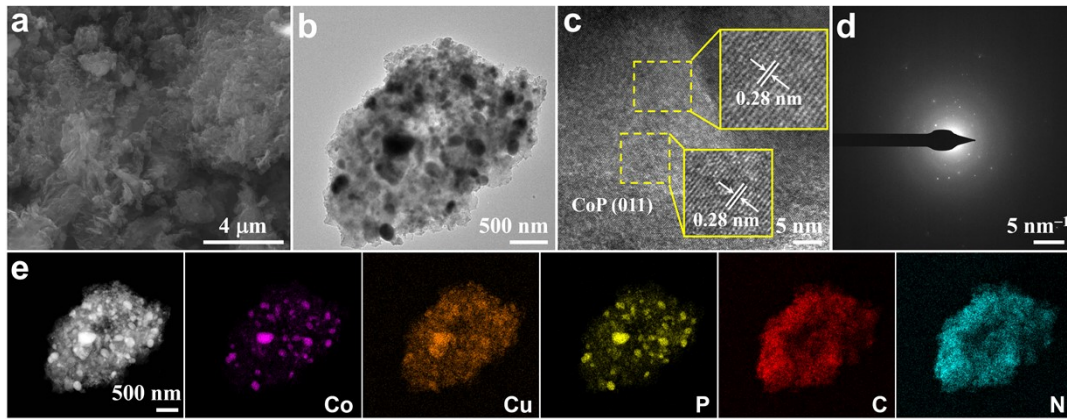


**Fig. S15.** Characterization after stability testing of CoP/Cu<sub>3</sub>P@NC. (a) SEM, (b) TEM, (c) HR-TEM, (d) SAED pattern, (e) HAADF-STEM and the corresponding elemental mapping images.

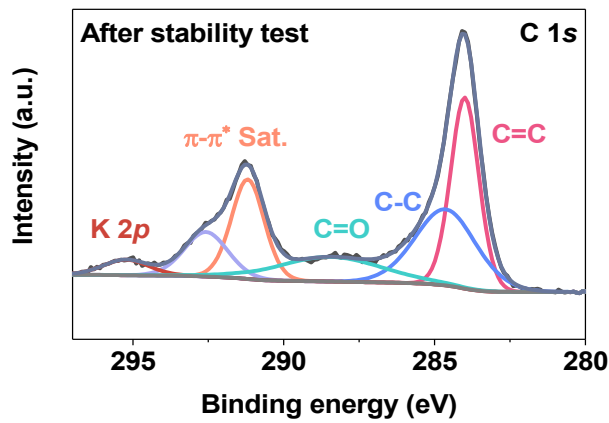


**Fig. S16.** High-resolution XPS spectrum of C 1s region in CoP/Cu<sub>3</sub>P@NC after ORR stability testing.

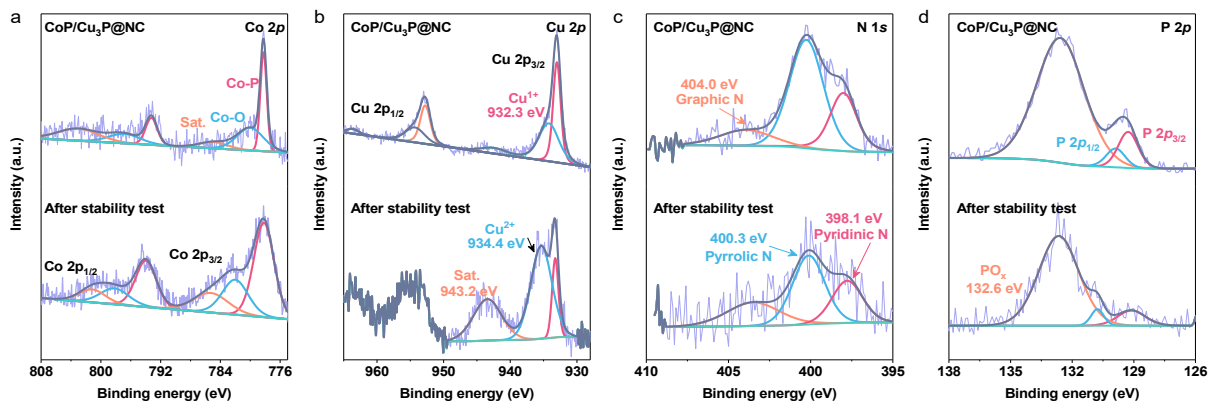


**Fig. S17.** High-resolution XPS spectra of CoP/Cu<sub>3</sub>P@NC before and after ORR stability testing.

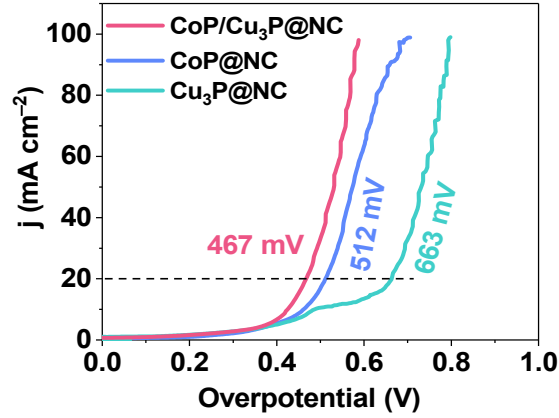


**Fig. S18.** LSV polarization curves of CoP/Cu<sub>3</sub>P@NC, CoP@NC, and Cu<sub>3</sub>P@NC in 1.0 M KOH solution for oxygen evolution reaction (OER).

**Table S1.** The percentage of atoms represented in the XPS spectra for the different catalysts.

Catalysts	Co	Cu	P	N	C
CoP/Cu <sub>3</sub> P@NC	<b>1.21</b>	<b>2.46</b>	<b>6.04</b>	<b>3.63</b>	<b>86.67</b>
CoP@NC	2.40	-	8.96	3.67	84.98
Cu <sub>3</sub> P@NC	-	1.62	4.03	5.12	89.23

**Table S2.** XPS peak fitting results of the prepared catalysts (%).

Catalysts	Co-O	Co-P	Cu <sup>+</sup>	Cu <sup>2+</sup>	P 2p <sub>3/2</sub>	P 2p <sub>1/2</sub>	P-O <sub>x</sub>
CoP/Cu <sub>3</sub> P@NC	<b>23.74</b>	<b>25.0</b>	<b>31.96</b>	<b>31.33</b>	<b>10.17</b>	<b>5.08</b>	<b>84.75</b>
CoP@NC	21.21	23.11	-	-	2.6	1.3	96.10
Cu <sub>3</sub> P@NC	-	-	29.70	28.33	2.47	1.45	96.08

**Table S3.** N 1s XPS peak fitting results of the prepared catalysts (%).

Catalysts	Pyridinic N	Pyrrolic N	Graphite N
CoP/Cu <sub>3</sub> P@NC	<b>39.5</b>	<b>49.35</b>	<b>11.15</b>
CoP@NC	18.01	70.82	11.17
Cu <sub>3</sub> P@NC	26.54	44.42	19.50

**Table S4.** Electrical conductivity of CoP/Cu<sub>3</sub>P@NC, CoP@NC and Cu<sub>3</sub>P@NC catalysts determined by four-point probe method.

Catalysts	Electrical resistivity ( $\Omega \text{ cm}^{-1}$ )	Electrical conductivity ( $\text{S cm}^{-1}$ )
CoP/Cu <sub>3</sub> P@NC	<b>39.8</b>	<b>25.13</b>
CoP@NC	47.0	21.28
Cu <sub>3</sub> P@NC	51.1	19.57

**Table S5.** Comparison of CoP/Cu<sub>3</sub>P@NC with previously reported for ORR electrocatalysts in 0.1 M KOH solution.

Catalysts	$E_{\text{onset}}$ (V vs. RHE)	Tafel ( $\text{mV dec}^{-1}$ )	Catalyst loading ( $\text{mg cm}^{-2}$ )	Reference
<b>CoP/Cu<sub>3</sub>P@NC</b>	<b>0.96</b>	<b>44</b>	<b>0.52</b>	<b>This work</b>
Cu/Zn-NC	0.89	54.8	0.392	3
Cu/Cu <sub>3</sub> P@NP-C-900	0.90	56.7	0.51	4
F-FeWO <sub>4</sub> /NC	~0.91	57.3	0.3469	5
Co/Zn@NCF	~0.89	40.5	0.214	6
Fe <sub>2</sub> P/NPC	0.997	86	0.86	7
CoP <sub>3</sub> /CeO <sub>2</sub> /C	0.802	58.0	0.2	8
CoP <sub>x</sub> @B-NPC	~0.91	72	0.16	9
Co <sub>3</sub> O <sub>4</sub> /N graphene	0.88	42	0.17	10
Co-SAs@NC	0.96	-	0.612	11
Ni-N <sub>4</sub> /GHSs/Fe-N <sub>4</sub>	~0.91	55	0.2551	12
Co/VN@NC	0.85	94	0.46	13
Co-Ni-SAs/NC	0.88	-	0.4	14
Co-NC-ADC	0.95	77.97	0.2038	15

**Table S6.** Comparison of CoP/Cu<sub>3</sub>P@NC with previously reported for aqueous ZAB.

Catalysts	OCV (V)	Peak power density ( $\text{mW cm}^{-2}$ )	Catalyst loading ( $\text{mg cm}^{-2}$ )	Reference
<b>CoP/Cu<sub>3</sub>P@NC</b>	<b>1.50</b>	<b>212.6</b>	<b>2</b>	<b>This work</b>
Cu/Cu <sub>3</sub> P@NP-C-900	1.42	148.2	5	4
Cu <sub>3</sub> P/MoP@C	1.51	156	1	16
CoP/NP-HPC	1.4	186	1	17
CoP/HNBs@NCL-2	1.51	139.8	1	18
CoP/CoO@MNC-CNT	-	152.8	2	19
Co <sub>x</sub> P@N,P-C	1.43	157	1	20
CoP/CoN@NCNRs/CC	1.515	120	-	21
CoP@NC-Ru	1.51	175	1.5	22
Co <sub>2</sub> P@NPC	1.43	157	5	23
CoP@Co <sub>2</sub> P/NPC-0.5	1.56	215.1	1.1	24
Ni <sub>x</sub> P-NP-C900	-	266	-	25

**Table S7.** Comparison of CoP/Cu<sub>3</sub>P@NC with previously reported for flexible ZAB.

Catalysts	OCV (V)	Peak power density (mW cm <sup>-2</sup> )	Catalyst loading (mg cm <sup>-2</sup> )	Reference
<b>CoP/Cu<sub>3</sub>P@NC</b>	<b>1.35</b>	<b>74</b>	<b>2 mg cm<sup>-2</sup></b>	<b>This work</b>
Co/N@CNTs@CNMF-800	1.40	26.5	-	26
CoNCNTF/CNF	1.34	63	-	27
FeCo-LCNT	1.425	62.0	1	28
7.1%Cu-Co <sub>2</sub> P@2D-NPC	1.42	51	1	29
Mn@Co-NS	1.36	64.80	5	30
CoCu/N-CNS-2	1.41	77.6	-	31

## References

1. L. Wang, J. Huang, X. Hu, Z. Huang, M. Gao, D. Yao, T. Taylor Isimjan and X. Yang, *J. Colloid Interface Sci.*, 2024, **660**, 989-996.
2. L. Wang, X. Hu, H. Li, Z. Huang, J. Huang, T. T. Isimjan and X. Yang, *Green Chem.*, 2024, **26**, 2011-2020.
3. M. Tong, F. Sun, Y. Xie, Y. Wang, Y. Yang, C. Tian, L. Wang and H. Fu, *Angew. Chem. Int. Ed.*, 2021, **60**, 14005-14012.
4. Y. Huang, F. Kong, F. Pei, L. Wang, X. Cui and J. Shi, *EcoMat*, 2023, **5**, e12335.
5. J.-C. Wu, X.-C. Shen, H. Wang, D.-J. Deng, S.-Q. Wu, Y. Gong, L.-H. Zhu, L. Xu and H.-N. Li, *Mater. Today Phys.*, 2023, **38**, 101274.
6. H. Pan, C. Zhang, Z. Lu, J. Dou, X. Huang, J. Yu, J. Wu, H. Li and X. Chen, *Chem. Eng. J.*, 2023, **477**, 147022.
7. L. Chen, Y. Zhang, L. Dong, X. Liu, L. Long, S. Wang, C. Liu, S. Dong and J. Jia, *Carbon*, 2020, **158**, 885-892.
8. J. Li, Y. Kang, Z. Lei and P. Liu, *Appl. Catal. B Environ. Energy*, 2023, **321**, 122029.
9. X. Shu, M. Yang, M. Liu, H. Wang and J. Zhang, *Chin. J. Catal.*, 2022, **43**, 3107-3115.
10. Y. Liang, Y. Li, H. Wang, J. Zhou, J. Wang, T. Regier and H. Dai, *Nat. Mater.*, 2011, **10**, 780-786.
11. X. Han, X. Ling, Y. Wang, T. Ma, C. Zhong, W. Hu and Y. Deng, *Angew. Chem. Int. Ed.*, 2019, **58**, 5359-5364.
12. J. Chen, H. Li, C. Fan, Q. Meng, Y. Tang, X. Qiu, G. Fu and T. Ma, *Adv. Mater.*, 2020, **32**, 2003134.
13. T. Cen, L. Qiu, Z. Ye, X. Peng, Y. Liu and D. Yuan, *Int. J. Hydrogen Energy*, 2021, **46**, 3337-3345.
14. X. Han, X. Ling, D. Yu, D. Xie, L. Li, S. Peng, C. Zhong, N. Zhao, Y. Deng and W. Hu, *Adv. Mater.*, 2019, **31**, 1905622.
15. Y. Feng, K. Song, W. Zhang, X. Zhou, S. J. Yoo, J.-G. Kim, S. Qiao, Y. Qi, X. Zou, Z. Chen, T. Qin, N. Yue, Z. Wang, D. Li and W. Zheng, *J. Energy Chem.*, 2022, **70**, 211-218.
16. M. Guo, M. Xu, Y. Qu, C. Hu, P. Yan, T. T. Isimjan and X. Yang, *Appl. Catal. B Environ. Energy*, 2021, **297**, 120415.
17. Y. Wang, M. Wu, J. Li, H. Huang and J. Qiao, *J. Mater. Chem. A*, 2020, **8**, 19043-19049.
18. B. Liu, X. Wang, R. Wang, G. Zhang, X. Xu, J. Liu, Z. Sun, M. Liu, C. Wang, X. Meng, J. Xie and J. Zou, *Chem. Eng. J.*, 2023, **475**, 146154.

19. H. W. Go, T. T. Nguyen, Q. P. Ngo, R. Chu, N. H. Kim and J. H. Lee, *Small*, 2023, **19**, 2206341.
20. Q. Shi, Q. Liu, Y. Zheng, Y. Dong, L. Wang, H. Liu and W. Yang, *Energy Environ. Mater.*, 2022, **5**, 515-523.
21. L. Bai, D. Wang, H. Shen, W. Wang, S. Li and W. Yan, *J. Mater. Chem. A*, 2024, **12**, 3997-4007.
22. M. M. Kumar, C. Aparna, A. K. Nayak, U. V. Waghmare, D. Pradhan and C. R. Raj, *ACS Appl. Mater. Interfaces*, 2024, **16**, 3542–3551.
23. H. Pan, X.-L. Wang, F. Li and Q. Xu, *J. Mater. Chem. A*, 2023, **11**, 15006-15013.
24. Z. Li, Y. Zeng, D. Xiong, L. Zhou, J. Zhou, Y. Yang, F. Zhan, K. Wang, Y. Du and Y. Liu, *Inorg. Chem. Front.*, 2024, **11**, 549-561.
25. Y. Wang, J. Liu, T. Lu, R. He, N. Xu and J. Qiao, *Appl. Catal. B Environ. Energy*, 2023, **321**, 122041.
26. T. Liu, J. Mou, Z. Wu, C. Lv, J. Huang and M. Liu, *Adv. Funct. Mater.*, 2020, **30**, 2003407.
27. D. Ji, L. Fan, L. Li, N. Mao, X. Qin, S. Peng and S. Ramakrishna, *Carbon*, 2019, **142**, 379-387.
28. Y. Deng, J. Zheng, B. Liu, Y. Liu, H. Li and M. Yang, *Carbon*, 2023, **210**, 118000.
29. L. Diao, T. Yang, B. Chen, B. Zhang, N. Zhao, C. Shi, E. Liu, L. Ma and C. He, *J. Mater. Chem. A*, 2019, **7**, 21232-21243.
30. X. Li, T. Zhou, Z. Luo, L. Zhang, Z. Ren, Q. Zhang, C. He, X. Jiang, Y. Li and X. Ren, *J. Alloys Compd.*, 2023, **939**, 168756.
31. J. Kuang, Y. Shen, Y. Zhang, J. Yao, J. Du, S. Yang, S. Zhang, Y. Fang and X. Cai, *Small*, 2023, **19**, 2207413.